

Two-orbital model for CeB₆

Dheeraj Kumar Singh*

Harish-Chandra Research Institute, Chhatnag Road, Jhansi, Allahabad 211019, India

We describe a two-orbital tight-binding model with bases belonging to the Γ_8 quartet. It captures several characteristics of the Fermiology unravelled by the recent angle-resolved photoemission spectroscopic (ARPES) measurements on cerium hexaboride CeB₆ samples cleaved along different high-symmetry crystallographic directions, which includes the ellipsoid-like Fermi surfaces (FSs) with major axes directed along Γ -X. We calculate various multipolar susceptibilities within the model and identify the susceptibility that shows the strongest divergence in the presence of standard onsite Coulomb interactions and discuss its possible implication and relevance with regard to the signature of strong ferromagnetic correlations existent in various phases as shown by the recent experiments.

PACS numbers: 71.27.+a, 75.25.Dk

I. INTRODUCTION

Strongly correlated f -electron systems exhibit a wide range of ordering phenomena including various magnetic orderings as well as superconductivity.^{1,2} However, they are notorious for possessing complex ordered phases or so called 'hidden order', which are sometimes not easily accessible experimentally because of the ordering of multipoles of higher rank such as electric quadrupolar, magnetic octupole etc. than the rank one magnetic dipole.^{3,4} This marked difference from the correlated d -electron system is a result of otherwise a strong spin-orbit coupling existent in these systems. Recent predictions of samarium hexaboride (SmB₆) to be a topological Kondo insulator has led to an intense interest and activities in these materials.⁵

CeB₆ with a simple cubic crystal structure is one of the most extensively studied f -electron system both theoretically as well as experimentally. Apart from the pronounced Kondo lattice properties, it undergoes two different types of ordering transition as a function of temperature despite its simple crystal structure.⁶ First, there is a transition to the AFQ phase with ordering wavevector $\mathbf{Q}_1 = (\pi, \pi, \pi)$ at $T_Q \approx 3.2K$, which has long remained hidden to the standard experimental probes such as neutron diffraction.⁷⁻¹¹ Then, another transition to the AFM phase with double \mathbf{Q}_2 commensurate structure with $\mathbf{Q}_2 = (\pi/2, \pi/2, 0)$ takes place at $T_N \approx 2.3K$.¹²

Significant progress has been made recently through the experiments in understanding the nature of above mentioned phases of CeB₆. Magnetic spin resonance, for instance, has been observed in the AFQ phase^{13,14} with its origin attributed to the ferromagnetic correlations^{15,16} as in the Yb compounds, e.g., YbRh,¹⁵ YbIr₂Si₂,¹⁷ and one Ce compound CeRuPO.¹⁸ On the other hand, according to a recent inelastic neutron-scattering (INS) experiment, AFM phase is rather a coexistence phase consisting of AFQ ordering as well.¹⁹ In another INS measurements, low-energy ferromagnetic fluctuations have been reported to be more intense than the mode corresponding to the magnetic ordering wavevector

\mathbf{Q}_2 in the AFM phase, which stays though with reduced intensity even in the pure AFQ phase.²⁰ Overall picture emerging from these experiments and hotspot observed near Γ by ARPES imply the existence of strong ferromagnetic fluctuations in various phases of CeB₆.

So far most of the theoretical studies have focused on the localized aspects of 4- f electron while neglecting the itinerant character when investigating multipole orderings.^{10,11,21} However, this may appear surprising because the estimates of density of states (DOS) for CeB₆ at the Fermi level from low-temperature specific heat measurement as well as from the effective mass measurement from de Haas-van Alphen (dHvA) gives a significantly larger value when compared to the paramagnetic metal such as LaB₆ provided that the FSs are considered same in both the compounds.²² In the temperature regime $T > T_Q$, it exhibits a typical dense Kondo behavior dominated by Fermi liquid with a Kondo temperature of the order of T_N and T_Q .²³ Moreover, a low energy dispersionless collective mode at \mathbf{Q}_1 has been observed in the INS experiments, which is well within the single particle charge gap present in the coexistence phase.¹⁹ The existence of such spin excitons have been reported in several superconductors²⁴ as well as heavy-fermion compounds²⁵ previously, and explanation for the origin of such modes has been provided in terms of correlated partilce-hole excitation a characteristics of the itinerant systems.

Recent advancement based on a full 3D tomographic sampling of the electronic structure by the APRES has unraveled the FSs in the high-symmetry planes of cubic CeB₆.^{26,27} FSs are found to be the cross sections of the ellipsoids, which exclude the Γ point and are bisected by (100) plane at $k_z = \pi$. The largest semi-principle axes of the ellipsoid coincides with Γ -X. Based on the FS characteristics, it has been suggested that multipole order may arise due to the nesting as the shifting of one ellipsoid by nesting vector (π, π, π) into the void formed in between other three can result in a significant overlap. Interestingly, the features of FS bear several similarities to those of LaB₆, which has also been suggested by earlier estimates based mainly on the dHvA experiments^{22,28} as

well as by several band-structure calculations.^{29–31}

Despite various experimental works on the FSs of CeB₆, no theoretical studies of ordering phenomena have been carried out within the models based on the realistic electronic structure, and therefore the nature of instability or fluctuations that will arise in that case is of strong current interest. To address this important issue, we propose to discuss a two-orbital tight-binding model with energy levels belonging to the Γ_8 quartet. The model reproduces the experimentally measured FSs well along the high-symmetry planes namely (100), (110) etc, which are part of the ellipsoid like three-dimensional FSs with the squarish cross sections. With this realistic electronic structure, we examine the nature of instability or fluctuations in the Hubbard-like model with standard onsite Coulomb interaction terms considered usually in a multi-orbital system such as iron-based superconductors. This is accomplished by studying behavior of the susceptibilities corresponding to the various multipolar moments.

II. MODEL HAMILTONIAN

Single particle state in the presence of strong spin-orbit coupling is defined by using total angular momentum $\mathbf{j} = \mathbf{l} + \mathbf{s}$, which yields low-lying sextet and high-lying octet for $j = 5/2$ and $7/2$, respectively in the case of f -electron with $l = 3$. Therefore, with the number of electrons n being 1, it is the low lying sextet, which is relevant in the case of Ce³⁺ ions. These ions are in the octahedral environment with corners being occupied by the six B ions. Therefore, the sextet is further split into Γ_8 quartet which forms the ground state of CeB₆ and a high lying Γ_7 doublet separated by $\sim 500K$. Γ_8 quartet involves two Kramers doublet and each doublet can be treated as spin- $\frac{1}{2}$ system.³²

Using Γ_8 quartet, kinetic part of our starting Hamiltonian is

$$\mathcal{H}_0 = \sum_{\mathbf{i}, \mathbf{j}} \sum_{\mu, \nu} \sum_{\sigma, \sigma'} t_{\mathbf{i}, \mathbf{j}}^{\mu\sigma; \nu\sigma'} (f_{\mathbf{i}\mu\sigma}^\dagger f_{\mathbf{j}\nu\sigma'} + \text{H.c.}), \quad (1)$$

where $t_{\mathbf{i}, \mathbf{j}}^{\mu\sigma; \nu\sigma'}$ are the hopping elements from orbital μ with pseudospin σ at site \mathbf{i} to orbital ν with pseudospin σ' at site \mathbf{j} . The operator $f_{\mathbf{i}\mu\sigma}^\dagger$ ($f_{\mathbf{i}\mu\sigma}$) creates (destroys) a f electron in the μ orbital of site \mathbf{i} with pseudo spin σ . These are given explicitly in terms of the z -components of the total angular momentum $j = 5/2$ as follows,

$$\begin{aligned} f_{i1\uparrow} &= \sqrt{\frac{5}{6}} c_{i-\frac{5}{2}} + \sqrt{\frac{1}{6}} c_{i\frac{3}{2}} \\ f_{i1\downarrow} &= \sqrt{\frac{5}{6}} c_{i\frac{5}{2}} + \sqrt{\frac{1}{6}} c_{i-\frac{3}{2}} \\ f_{i2\uparrow} &= c_{i-\frac{1}{2}}, \quad f_{i2\downarrow} = c_{i\frac{1}{2}}. \end{aligned} \quad (2)$$

As can be seen in Fig. 1, Γ_8 orbitals are similar in structure to the d -orbitals $d_{x^2-y^2}$ and $d_{3z^2-r^2}$.



FIG. 1. $\Gamma_{8(1)}$ and $\Gamma_{8(2)}$ orbitals with a similar structure as d -orbitals $d_{x^2-y^2}$ and $d_{3z^2-r^2}$, respectively.

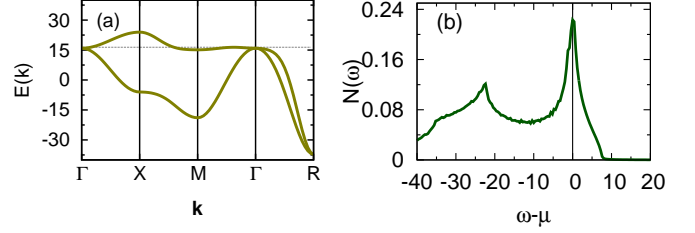


FIG. 2. (a) Electron dispersions along high-symmetry direction Γ -X-M- Γ -R and (b) DOS, which is peaked near the Fermi level.

Kinetic energy after the Fourier transform can be expressed in terms of Γ matrices defined as $\hat{\Gamma}^{0,1,2,3,4,5} = (\hat{\tau}_0\hat{\sigma}_0, \hat{\tau}_z\hat{\sigma}_0, \hat{\tau}_x\hat{\sigma}_0, \hat{\tau}_y\hat{\sigma}_0, \hat{\tau}_y\hat{\sigma}_x, \hat{\tau}_y\hat{\sigma}_y, \hat{\tau}_y\hat{\sigma}_z)$, where σ_i s and τ_i s are Pauli's matrices corresponding to the spin and orbital degrees of freedom, respectively. So that

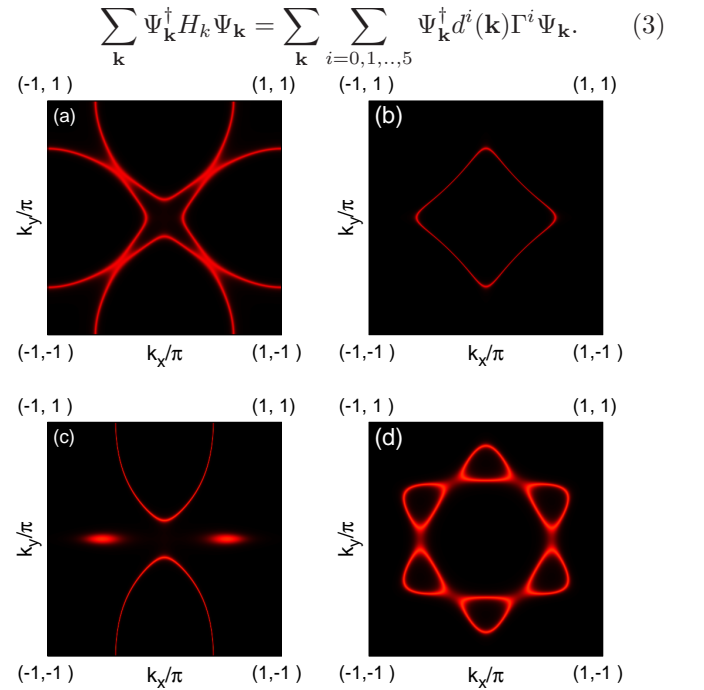


FIG. 3. Electron dispersions along high-symmetry plane (a) (100), (b) at π along (100), (c) (110) and (d) (111) obtained for the chemical potential $\mu = 16.4$.

Here, $\Psi_{\mathbf{k}}^{\dagger} = (f_{\mathbf{k}1\uparrow}^{\dagger}, f_{\mathbf{k}2\uparrow}^{\dagger}, f_{\mathbf{k}1\downarrow}^{\dagger}, f_{\mathbf{k}2\downarrow}^{\dagger})$ is the electron field with $d^i(\mathbf{k})$ s

$$\begin{aligned}
d^0(\mathbf{k}) &= -\mu + 8t\phi_0(\mathbf{k}) + \frac{28}{3}t'\phi'_0(\mathbf{k}) + \frac{128}{9}t''\phi''_0(\mathbf{k}) \\
d^1(\mathbf{k}) &= 4t\phi_1(\mathbf{k}) - \frac{2}{3}t'\phi'_1(\mathbf{k}) \\
d^2(\mathbf{k}) &= -4\sqrt{3}t\phi_2(\mathbf{k}) + \frac{2}{\sqrt{3}}t'\phi'_2(\mathbf{k}) \\
d^3(\mathbf{k}) &= \frac{16}{\sqrt{3}}t'\phi'_3(\mathbf{k}) + \frac{128}{9\sqrt{3}}t''\phi''_3(\mathbf{k}) \\
d^4(\mathbf{k}) &= \frac{16}{\sqrt{3}}t'\phi'_4(\mathbf{k}) + \frac{128}{9\sqrt{3}}t''\phi''_4(\mathbf{k}) \\
d^5(\mathbf{k}) &= \frac{16}{\sqrt{3}}t'\phi'_5(\mathbf{k}) + \frac{128}{9\sqrt{3}}t''\phi''_5(\mathbf{k}).
\end{aligned} \tag{4}$$

t' and t'' are the second and third next-nearest neighbor hopping parameters. Various $\phi(\mathbf{k})$ s are expressed in terms of cosines and sines of the components of momentum in the Brillouin zone as

$$\begin{aligned}
\phi_0 &= \cos k_x + \cos k_y + \cos k_z \\
\phi'_0 &= \cos k_y \cos k_z + \cos k_z \cos k_x + \cos k_x \cos k_y \\
\phi_1 &= \cos k_x + \cos k_y - 2 \cos k_z \\
\phi'_1 &= \cos k_y \cos k_z + \cos k_z \cos k_x - 2 \cos k_x \cos k_y \\
\phi_2 &= \cos k_x - \cos k_y \\
\phi'_2 &= \cos k_y \cos k_z - \cos k_z \cos k_x \\
\phi'_3 &= \sin k_y \sin k_z \\
\phi'_4 &= \sin k_z \sin k_x \\
\phi'_5 &= \sin k_x \sin k_y \\
\phi''_0 &= \cos k_x \cos k_y \cos k_z \\
\phi''_3 &= \cos k_x \sin k_y \sin k_z \\
\phi''_4 &= \sin k_x \cos k_y \sin k_z \\
\phi''_5 &= \sin k_x \sin k_y \cos k_z.
\end{aligned} \tag{5}$$

In the absence of the second and third nearest-neighbor hopping, the kinetic part of the Hamiltonian reduces to that of manganites³³ with the only difference of a constant multiplication factor. In the following, the unit of energy is set to be t . Calculated electron dispersions for $t' = -0.38$ and $t'' = 0.18$, which consists of doubly degenerate eigenvalues, are shown in Fig. 3(a) along the high symmetry directions. A large hole pocket near X and the extrema exhibited by two bands near Γ just below the Fermi level are broadly in agreement with 4f dominated part in the band-structure calculations. The density of states (DOS) show two peaks with larger one being in the vicinity of the Fermi level (Fig. 3(b)). It is not unexpected particularly because of the flatness of the two bands near Γ contributing mostly to the DOS at the Fermi level. Interestingly, a hot spot near Γ has been observed also in the ARPES measurements, which points towards the possibility of strong ferromagnetic fluctuations.²⁷ Here, the chemical potential is chosen to be 16.4 to obtain a better agreement with the ARPES FSs.

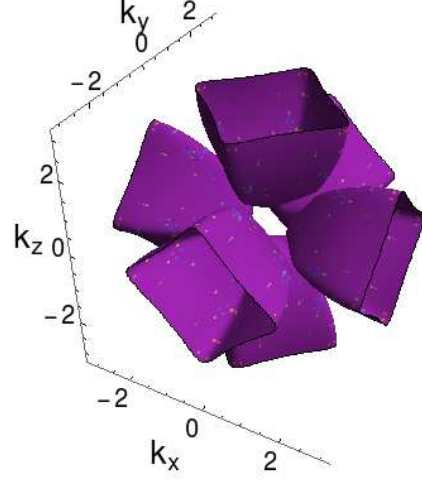


FIG. 4. Fermi surfaces in the Brillouin zone for the chemical potential $\mu = 16.4$.

Fig. 3 shows FSs cut along different high-symmetry planes. It has an ellipse-like structure with major axis aligned along Γ -X for the (100) plane while touching each other along Γ -M direction. On the other hand, the parallel plane at $(0, 0, \pi)$ consists of a single squarish pocket around that point. In the absence of four-fold rotation symmetry for the (110) plane, two large ellipse-like FSs are present with the major axes along Γ -Y direction while small pockets exist along Γ -X direction. The six-fold rotation symmetry is reflected by the six pockets along (111) plane. All of them are obtained from the FSs shown in the whole Brillouin zone as in the Fig. 3. It consists of an ellipsoid-like FSs with largest semi-principal axes coinciding with Γ -X, however, with a squarish cross section. An overall good agreement exists with the several recent ARPES measurements.^{26,27} ARPES estimates are believed to more reliable when compared with the earlier estimates from dHvA experiments carried out in the presence of magnetic field as the latter has the potential to affect the hot spots.

III. MULTIPOLAR SUSCEPTIBILITIES

Sixteen multipolar moments can be defined for the Γ_8 state including one charge, three dipole, five quadrupole and seven octapole, which are rank-0, rank-1, rank-2 and rank-3 tensors, respectively. The dipole belongs to the Γ_4^- irreducible representation, where $-$ sign denote the breaking of time reversal symmetry. It's components are given by the outer product of Pauli's matrices $\hat{\tau}_i \hat{\sigma}_i$ s. The quadrupole moments belonging to Γ_3^+ are $\hat{\tau}_x \hat{\sigma}_0$ and $\hat{\tau}_z \hat{\sigma}_0$ while those belonging to Γ_5^+ irreducible representations are expressed as $\hat{\tau}_i \hat{\sigma}_y$ s. The octapolar moments with Γ_2^- representation is $\hat{\tau}_y \hat{\sigma}_0$, whereas the z -component of those belonging to Γ_4^- and Γ_5^- are $2\hat{\tau}_z \hat{\sigma}_z$ and $2\hat{\tau}_x \hat{\sigma}_z$, respectively.

In order to examine the multipolar ordering instabil-

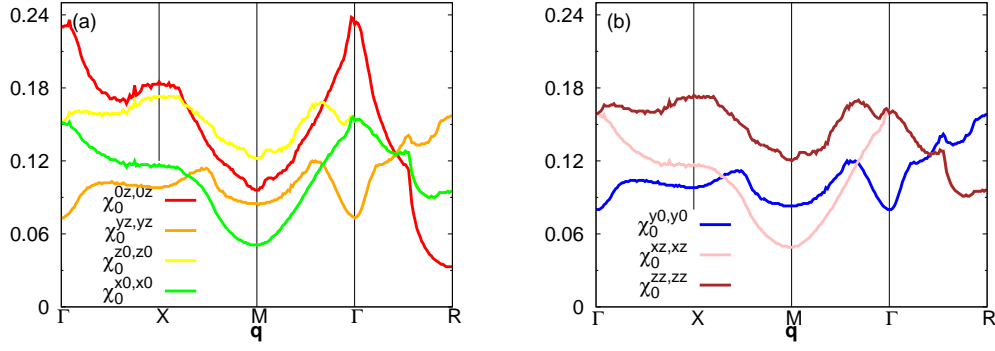


FIG. 5. (a) Magnetic and quadrupolar static susceptibilities along high-symmetry direction Γ -X-M- Γ -R. (b) Octapolar static susceptibilities.

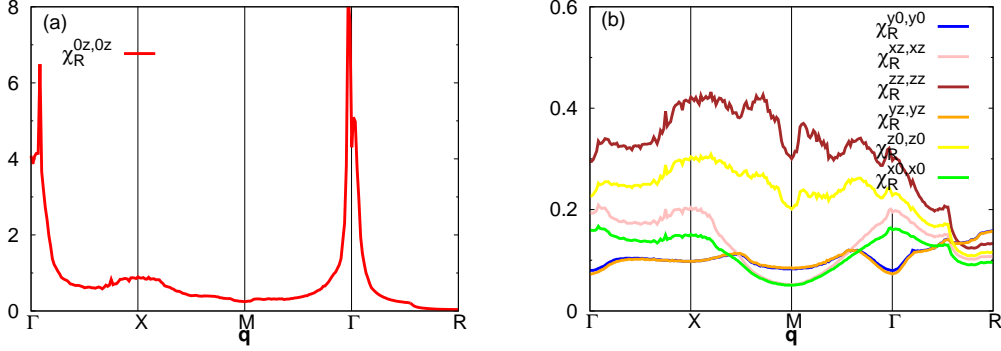


FIG. 6. Multipolar static susceptibilities calculated at the RPA-level for $U = 15$ and $J = 0.16U$. (a) Spin susceptibility diverges near $(0, 0, 0)$. (b) For the same set of interaction parameters quadrupolar and octapolar susceptibilities are divergenceless.

ities, we calculate susceptibilities while considering only the z -component whenever component along three coordinate axes are present as that will be sufficient because of the cubic symmetry. Multipolar susceptibilities are defined as³⁴

$$\chi^{pq,rs}(\mathbf{q}, i\omega_n) = \frac{1}{\beta} \int_0^\beta d\tau e^{i\omega_n \tau} \langle T_\tau [\mathcal{O}_\mathbf{q}^{pq}(\tau) \mathcal{O}_{-\mathbf{q}}^{rs}(0)] \rangle, \quad (6)$$

where

$$\mathcal{O}_\mathbf{q}^{pq} = \sum_{\mathbf{k}} \sum_{\sigma\sigma'} \sum_{\mu\mu'} f_{\mu\sigma}^\dagger(\mathbf{k} + \mathbf{q}) \tau_{\mu\mu'}^p \sigma_{\sigma\sigma'}^q f_{\mu'\sigma'}(\mathbf{k}). \quad (7)$$

They can be expressed in terms of

$$\begin{aligned} \chi_{\mu_1\mu_2;\mu_4\mu_3}^{\sigma_1\sigma_2;\sigma_4\sigma_3}(\mathbf{q}, i\omega_n) &= \frac{1}{\beta} \int_0^\beta d\tau \sum_{\mathbf{k}, \mathbf{k}'} \langle T_\tau f_{\mathbf{k}+\mathbf{q}\mu_1\sigma_1}^\dagger(\tau) f_{\mathbf{k}\mu_2\sigma_2}(\tau) \\ &\times f_{\mathbf{k}'-\mathbf{q}\mu_3\sigma_3}^\dagger(0) f_{\mathbf{k}'\mu_4\sigma_4}(0) \rangle \end{aligned} \quad (8)$$

which form a 16×16 matrix. Thus, the dipole or spin susceptibility is given by

$$\chi^{0z,0z}(\mathbf{q}, i\omega_n) = \sum_{\sigma\sigma'} \sum_{\mu\mu'} \sigma\sigma' \chi_{\mu\mu';\mu'\mu'}^{\sigma\sigma;\sigma'\sigma'}(\mathbf{q}, i\omega_n), \quad (9)$$

where σ and μ in front of χ takes $+1$ or -1 corresponding to the two spin or orbital degrees of freedom. Various

quadrupolar and octapolar susceptibilities are given as

$$\begin{aligned} \chi^{x0,x0}(\mathbf{q}, i\omega_n) &= \sum_{\sigma} \sum_{\mu\mu'} \chi_{\mu\bar{\mu};\mu'\bar{\mu}'}^{\sigma\sigma;\sigma\sigma'}(\mathbf{q}, i\omega_n) \\ \chi^{z0,z0}(\mathbf{q}, i\omega_n) &= \sum_{\sigma} \sum_{\mu\mu'} \mu\mu' \chi_{\mu\mu;\mu'\mu'}^{\sigma\sigma;\sigma\sigma'}(\mathbf{q}, i\omega_n) \\ \chi^{yz,yz}(\mathbf{q}, i\omega_n) &= -i^2 \sum_{\sigma\sigma'} \sum_{\mu\mu'} \sigma\sigma' \mu\mu' \chi_{\mu\bar{\mu};\mu'\bar{\mu}'}^{\sigma\sigma;\sigma'\sigma'}(\mathbf{q}, i\omega_n) \end{aligned} \quad (10)$$

and

$$\begin{aligned} \chi^{y0,y0}(\mathbf{q}, i\omega_n) &= -i^2 \sum_{\sigma} \sum_{\mu\mu'} \mu\mu' \chi_{\mu\bar{\mu};\mu'\bar{\mu}'}^{\sigma\sigma;\sigma\sigma'}(\mathbf{q}, i\omega_n) \\ \chi^{xz,xz}(\mathbf{q}, i\omega_n) &= \sum_{\sigma\sigma'} \sum_{\mu\mu'} \sigma\sigma' \chi_{\mu\bar{\mu};\mu'\bar{\mu}'}^{\sigma\sigma;\sigma'\sigma'}(\mathbf{q}, i\omega_n) \\ \chi^{zz,zz}(\mathbf{q}, i\omega_n) &= \sum_{\sigma\sigma'} \sum_{\mu\mu'} \sigma\sigma' \mu\mu' \chi_{\mu\mu;\mu'\mu'}^{\sigma\sigma;\sigma'\sigma'}(\mathbf{q}, i\omega_n), \end{aligned} \quad (11)$$

respectively.

Fig. 5 shows different static multipolar susceptibilities with well-defined peaks for some while broad hump like structure for the other. Particularly, the spin susceptibility $\bar{\chi}^{0z,0z}$ is, among all, sharply peaked, however, at $\approx \mathbf{Q}_3 = (0, 0, 0)$. Quadrupolar susceptibility $\bar{\chi}^{yz,yz}$ corresponding to the AFQ order observed in experiments, on the other hand, does show a peak near \mathbf{Q}_1 . Other quadrupolar susceptibility $\bar{\chi}^{x0,x0}$ is peaked near \approx

\mathbf{Q}_3 while $\bar{\chi}^{z0,z0}$ has a broad hump like structure near $(\pi, 0, 0)$ and a peak slightly away from $(\pi/2, \pi/2, \pi/2)$. We further note that $\bar{\chi}^{x0,x0} = \bar{\chi}^{xz,xz}$, $\bar{\chi}^{y0,y0} = \bar{\chi}^{yz,yz}$ and $\bar{\chi}^{z0,z0} = \bar{\chi}^{zz,zz}$ as shown in Fig. 5(b)

IV. MULTIPOLAR SUSCEPTIBILITIES IN THE PRESENCE OF INTERACTION

In order to investigate the role of electron-electron correlation, we consider the standard onsite Coulomb interaction terms given as

$$\begin{aligned} \mathcal{H}_{int} = & U \sum_{\mathbf{i}, \mu} n_{\mathbf{i}\mu\uparrow} n_{\mathbf{i}\mu\downarrow} + (U' - \frac{J}{2}) \sum_{\mathbf{i}, \mu < \nu} n_{\mathbf{i}\mu} n_{\mathbf{i}\nu} \\ & - 2J \sum_{\mathbf{i}, \mu < \nu} \mathbf{S}_{\mathbf{i}\mu} \cdot \mathbf{S}_{\mathbf{i}\nu} + J \sum_{\mathbf{i}, \mu < \nu, \sigma} f_{\mathbf{i}\mu\sigma}^\dagger f_{\mathbf{i}\mu\bar{\sigma}}^\dagger f_{\mathbf{i}\nu\bar{\sigma}} f_{\mathbf{i}\nu\sigma}, \end{aligned} \quad (12)$$

in a manner similar to the various correlated multiorbital systems. First term represents the intraorbital Coulomb interaction for each orbital. Second and third term represent the density-density interaction and Hund's coupling between the two orbitals. Fourth term represents the pair-hopping energy whereas the condition $U' = U - 2J$ is essential for the rotational invariance.

Multipolar susceptibilities in the presence of interaction can be obtained from Dyson's equation yielding

$$\hat{\chi}_R(\mathbf{q}, i\omega) = (\hat{\mathbf{1}} - \hat{U} \hat{\chi}(\mathbf{q}, i\omega))^{-1} \hat{\chi}(\mathbf{q}, i\omega). \quad (13)$$

Here, $\hat{\mathbf{1}}$ is a 16×16 identity matrix, whereas the interaction matrix is given by³⁵

$$U_{\mu_1\mu_2;\mu_3\mu_4}^{\sigma_1\sigma_2;\sigma_3\sigma_4} = \begin{cases} -U & (\mu_1 = \mu_2 = \mu_3 = \mu_4, \sigma_1 = \sigma_2 \neq \sigma_3 = \sigma_4) \\ -U' & (\mu_1 = \mu_2 \neq \mu_3 = \mu_4, \sigma_1 = \sigma_2 \neq \sigma_3 = \sigma_4) \\ -J & (\mu_1 = \mu_4 \neq \mu_2 = \mu_3, \sigma_1 = \sigma_2 \neq \sigma_3 = \sigma_4) \\ -J' & (\mu_1 = \mu_3 \neq \mu_2 = \mu_4, \sigma_1 = \sigma_2 \neq \sigma_3 = \sigma_4) \\ -(U - J') & (\mu_1 = \mu_2 \neq \mu_3 = \mu_4, \sigma_1 = \sigma_2 = \sigma_3 = \sigma_4) \\ (U - J') & (\mu_1 = \mu_4 \neq \mu_2 = \mu_3, \sigma_1 = \sigma_2 = \sigma_3 = \sigma_4) \\ U & (\mu_1 = \mu_2 = \mu_3 = \mu_4, \sigma_1 = \sigma_4 \neq \sigma_2 = \sigma_3) \\ U' & (\mu_1 = \mu_4 \neq \mu_2 = \mu_3, \sigma_1 = \sigma_4 \neq \sigma_2 = \sigma_3) \\ J & (\mu_1 = \mu_2 \neq \mu_3 = \mu_4, \sigma_1 = \sigma_4 \neq \sigma_2 = \sigma_3) \\ J' & (\mu_1 = \mu_3 \neq \mu_2 = \mu_4, \sigma_1 = \sigma_4 \neq \sigma_2 = \sigma_3) \\ 0 & (\text{otherwise}) \end{cases}. \quad (14)$$

Fig. 6 show the multipolar static susceptibilities at the RPA-level. As expected, the RPA spin susceptibility requires the smallest critical interaction strength $U = 15$ ($U/W < 1/3$) with $J = 0.16U$ to show the divergence. Interestingly, it diverges near \mathbf{Q}_3 instead of at the AFM

ordering wave vector \mathbf{Q}_2 , which is not surprising because there exists a large DOS near Γ that leads also to the peak near \mathbf{Q}_3 in bare spin susceptibility. Thus, AFQ instability corresponding to the Γ_5^+ representation is absent in the model despite the bare quadrupole susceptibility being peaked near \mathbf{Q}_1 . However, we believe that the strong low-energy ferromagnetic fluctuations in the paramagnetic phase may have important implications for the persistent ferromagnetic correlations in various ordered phases as observed by various experiments.^{14,20}

V. CONCLUSIONS AND DISCUSSIONS

In conclusions, we have described a tight-binding model with the bases as Γ_8 , which captures the salient features of the Fermi surfaces along the high-symmetry planes as observed in the ARPES measurements. A large density of state is obtained near the Fermi level due to the flatness of the bands close to Γ , which bears a remarkable similarity to the hot-spot observed in another ARPES experiments. Multipolar susceptibilities calculated with the standard onsite Coulomb interactions as in other multiorbital systems show that it is the spin susceptibility that exhibits strongest diverging behavior. Moreover, it does so in the low-momentum region implying an underlying ferromagnetic instability.

It is clear that nature of the instability obtained with the realistic electronic structure is different from the actual order in CeB_6 . However, it is important to note that some of the recent experiments have provided the evidence of strong ferromagnetic correlations in the ordered phases. For instance, there exists magnetic spin resonance in the AFQ phase, which has been attributed to the FM correlations. Further, the most intense spin-wave excitation modes have been observed at zero-momentum instead of the AFM ordering wavevector by the INS measurements in the coexistence phase, which continues to be present even in the AFQ phase. A similar INS measurement in the paramagnetic phase is highly desirable to probe the existence of ferromagnetic correlations in the paramagnetic phase. So far only an indirect indication in the form of hot-spot observed by ARPES near Γ is available. In order to understand above mentioned features, we believe that the strong low-energy ferromagnetic fluctuations obtained within the two-orbital model with the realistic electronic structure may be an important step. To explain AFQ and other multipole order, it would perhaps be necessary to include the local-exchange terms involving AFQ and multipolar moments. Such a proposal should be the subject matter of future investigation in order to describe various complex ordering phenomena as well as associated unusual features within a single model.

We acknowledge the use of HPC clusters at HRI.

-
- * dheerajsingh@hri.res.in
- ¹ J. A. Mydosh and P. M. Oppeneer, Colloquium: hidden order, superconductivity, and magnetism—the unsolved case of URu₂Si₂, *Rev. Mod. Phys.* **83**, 1301 (2011).
 - ² P. Thalmeier, T. Takimoto, J. Chang, and I. Eremin, *J. Phys. Soc. Jpn.* **77**, 43 (2008).
 - ³ Y. Kuramoto, H. Kusunose, and A. Kiss, *J. Phys. Soc. Jpn.* **78**, 072001 (2009).
 - ⁴ P. Santini, *Rev. Mod. Phys.* **81**, 807 (2009).
 - ⁵ T. Takimoto, *J. Phys. Soc. Jpn.* **80** 123710 (2011).
 - ⁶ T. Kasuya, K. Takegahara, Y. Aoki, T. Suzuki, S. Kunii, M. Sera, N. Sato, T. Fujita., T. Goto., A. Tamaki, and T. Komatsubara, in: *Proc. Intern. Conf. on Valence Instabilities*, eds. P. Wachter and H. Boppert, 359 (North-Holland, Amsterdam, 1982).
 - ⁷ J. M. Effantin, J. Rossat-Mignod, P. Burlet, H. Bartholin, S. Kunii and T. Kasuya, *J. Magn. Magn. Mater.* **4748** 145148 (1985).
 - ⁸ R. G. Goodrich, D. P. Young, D. Hall, L. Balicas, Z. Fisk, N. Harrison, J. Betts, A. Migliori, F. M. Woodward, and J. W. Lynn, *Phys. Rev. B* **69**, 054415 (2004).
 - ⁹ T. Matsumura, T. Yonemura, K. Kunimori, M. Sera, F. Iga, T. Nagao, and J.-I. Igarashi, *Phys. Rev. B* **85**, 174417 (2012).
 - ¹⁰ R. Shiina, H. Shiba, P. Thalmeier, A. Takahashi, and O. Sakai, *J. Phys. Soc. Jpn.* **72**, 1216 (2003).
 - ¹¹ P. Thalmeier, R. Shiina, H. Shiba, A. Takahashi, and O. Sakai, *J. Phys. Soc. Jpn.* **72**, 3219 (2003).
 - ¹² O. Zaharko, P. Fischer, A. Schenck, S. Kunii, P.-J. Brown, F. Tasset, and T. Hansen, *Phys. Rev. B* **68**, 214401 (2003).
 - ¹³ S. V. Demisheva, A. V. Semenoa, A. V. Bogacha, Yu. B. Padernob, N. Yu. Shitsevalovab, N. E. Sluchankoa, *J. Magn. Magn. Mater.* **300**, e534-e537 (2006).
 - ¹⁴ S. V. Demishev, A. V. Semeno, A. V. Bogach, N. A. Samarin, T. V. Ishchenko, V. B. Filipov, N. Yu. Shitsevalova, and N. E. Sluchanko, *Phys. Rev. B* **80**, 245106 (2009).
 - ¹⁵ C. Krellner, T. Förster, H. Jeevan, C. Geibel, and J. Sichelschmidt, *Phys. Rev. Lett.* **100**, 066401 (2008).
 - ¹⁶ P. Schlottmann, *Phys. Rev. B* **86**, 075135 (2012).
 - ¹⁷ J. Sichelschmidt, J. Wykhoff, H.-A. Krug von Nidda, I. I. Fazlishanov, Z. Hossain, C. Krellner, C. Geibel, and F. Steglich, *J. Phys.: Condens. Matter* **19**, 016211 (2007).
 - ¹⁸ E. M. Bruning, C. Krellner, M. Baenitz, A. Jesche, F. Steglich, and C. Geibel, *Phys. Rev. Lett.* **101**, 117206 (2008).
 - ¹⁹ G. Friemel, Y. Li, A. V. Dukhnenko, N. Y. Shitsevalova, N. E. Sluchanko, A. Ivanov, V. B. Filipov, B. Keimer, and D.S. Inosov, *Nat. Comm.* **3**, 830 (2012).
 - ²⁰ H. Jang, G. Friemel, J. Ollivier, A. V. Dukhnenko, N. Yu. Shitsevalova, V. B. Filipov, B. Keimer, and D. S. Inosov, *Nat. Mat.* **13**, 682 (2014).
 - ²¹ F. J. Okhawa, *J. Phys. Soc. Jpn.* **54**, 3909 (1985).
 - ²² N. Harrison, P. Meson, P.-A. Probst, and M. Springford, *J. Phys.: Condens. Matter* **5** 7435 (1993).
 - ²³ S. Nakamura, T. Goto, and S. Kunii, *J. Phys. Soc. Jpn.* **64**, 3941 (1995).
 - ²⁴ I. Eremin, G. Zwicknagl, P. Thalmeier, and P. Fulde, *Phys. Rev. Lett.* **101**, 187001 (2008).
 - ²⁵ A. Akbari and P. Thalmeier, *Phys. Rev. Lett.* **108**, 146403 (2012).
 - ²⁶ A. Koitzsch, N. Heming, M. Knupfer, B. Büchner, P. Y. Portnichenko, A. V. Dukhnenko, N. Y. Shitsevalova, V. B. Filipov, L. L. Lev, V. N. Strocov, J. Ollivier, and D. S. Inosov, *Nat. Comm.* **7** 10876 (2016).
 - ²⁷ M. Neupane, N. Alidoust, I. Belopolski, G. Bian, S.-Y. Xu, Dae-Jeong Kim, P. P. Shibayev, D. S. Sanchez, H. Zheng, T.-R. Chang, H.-T. Jeng, P. S. Riseborough, H. Lin, A. Bansil, T. Durakiewicz, Z. Fisk, and M. Z. Hasan, *Phys. Rev. B* **92**, 104420 (2015).
 - ²⁸ Y. Ōnuki, T. Komatsubara, P. H. P. Reinders, and M. Springford, *J. Phys. Soc. Jpn.* **58**, 3698 (1989).
 - ²⁹ T. Kasuya and H. Harima, *J. Phys. Soc. Jpn.* **65**, 3698 (1996).
 - ³⁰ M. B. Suvasini, G. Y. Guo, W. M. Temmerman, G. A. Gehring, and M. Biasini, *J. Phys.: Condens. Matter* **8** 7105-7125 (1996).
 - ³¹ N. Singh, S. M. Saini, T. Nautiyal and S. Auluck, *J. Phys.: Condens. Matter* **19** (2007) 346226.
 - ³² T. Hotta and K. Ueda, *Phys. Rev. B* **67**, 104518 (2003).
 - ³³ E. Dagotto, T. Hotta, and A. Moreoa, *Phys. Rep.* **344** 1 (2001).
 - ³⁴ T. Takimoto, T. Hotta, T. Maehira, and K. Ueda, *J. Phys.: Condens. Matter* **14** (2002) L369-L375.
 - ³⁵ D. D. Scherer, I. Eremin, and B. M. Andersen, *Phys. Rev. B* **94**, 180405 (2016).